Addiction Biology

SSA SOCIETY FOR THE STUDY OF ADDICTION

ORIGINAL ARTICLE

doi:10.1111/adb.12418

Multi-modal MRI classifiers identify excessive alcohol consumption and treatment effects in the brain

Alejandro Cosa[1,2,†], Andrea Moreno[1], Jesús Pacheco-Torres[1], Roberto Ciccocioppo[3], Petri Hyytiä[4], Wolfgang H. Sommer[5], David Moratal[2] & Santiago Canals[1]

Instituto de Neurociencias, Consejo Superior de Investigaciones Científicas and Universidad Miguel Hernández, Sant Joan d'Alacant, Spain[1], Center for Biomaterials and Tissue Engineering, Universitat Politècnica de València, Valencia, Spain[2], School of Pharmacy University of Camerino, Camerino, Italy[3], Department of Pharmacology, Faculty of Medicine, University of Helsinki, Helsinki Finland[4] and Department of Psychopharmacology, Central Institute of Mental Health, University of Heidelberg, Mannheim, Germany[5]

ABSTRACT

Robust neuroimaging markers of neuropsychiatric disorders have proven difficult to obtain. In alcohol use disorders, profound brain structural deficits can be found in severe alcoholic patients, but the heterogeneity of unimodal MRI measurements has so far precluded the identification of selective biomarkers, especially for early diagnosis. In the present work we used a combination of multiple MRI modalities to provide comprehensive and insightful descriptions of brain tissue microstructure. We performed a longitudinal experiment using Marchigian–Sardinian (msP) rats, an established model of chronic excessive alcohol consumption, and acquired multi-modal images before and after 1 month of alcohol consumption (6.8 ± 1.4 g/kg/day, mean ± SD), as well as after 1 week of abstinence with or without concomitant treatment with the antirelapse opioid antagonist naltrexone (2.5 mg/kg/day). We found remarkable sensitivity and selectivity to accurately classify brains affected by alcohol even after the relative short exposure period. One month drinking was enough to imprint a highly specific signature of alcohol consumption. Brain alterations were regionally specific and affected both gray and white matter and persisted into the early abstinence state without any detectable recovery. Interestingly, naltrexone treatment during early abstinence resulted in subtle brain changes that could be distinguished from non-treated abstinent brains, suggesting the existence of an intermediate state associated with brain recovery from alcohol exposure induced by medication. The presented framework is a promising tool for the development of biomarkers for clinical diagnosis of alcohol use disorders, with capacity to further inform about its progression and response to treatment.

Keywords alcohol use disorders, classification algorithms, machine learning, multi-modal MRI, naltrexone, rat.

Correspondence to: David Moratal, Center for Biomaterials and Tissue Engineering, Universitat Politècnica de València, 46022 Valencia, Spain. E-mail: dmoratal@eln.upv.es Santiago Canals, Instituto de Neurociencias Consejo Superior de Investigaciones Científicas—Universidad Miguel Hernández, Campus de Sant Joan, Apt. 18\ 03550 Sant Joan d'Alacant, Alicante, Spain. E-mail: scanals@umh.es

INTRODUCTION

Alcohol abuse is one of the most alarming problems for our health systems. About 10 percent of the total burden of disease in developed countries is caused by alcohol use alone (Whiteford *et al.* 2013). Only in the European Community, nearly 60 million citizens engage in harmful consumption patterns and 23 million are estimated to suffer from alcohol addiction (Wittchen *et al.* 2011). While many factors are contributing to the unsuccessful efforts to limit heavy drinking, one important problem is the detection of alcohol use disorders (AUDs) at early stages.

Relevant information to assist diagnosis is often obtained from non-invasive neuroimaging, notably MRI. In alcohol-dependent patients, severe chronic drinking has been related to reductions in white and gray matter volume in frontal cortex (Bühler & Mann 2011; Demirakca *et al.* 2011; Kril *et al.* 1997; Rando *et al.* 2011) and gray-matter in limbic areas (Fein *et al.* 2006; Makris *et al.* 2008), as well as alteration in the resting-state functional connectivity of some frontal cortical regions, such as the anterior cingulate cortex (Muller-Oehring *et al.* 2015), to mention some examples. While these studies have provided highly valuable information

[†]Present address: Central Institute of Mental Health University of Heidelberg Mannheim Germany

at the group level to help understanding the pathology in AUDs, the large heterogeneity found across subjects and disease severity in the degree of alcohol related brain damage, as characterized by single MRI modalities, has precluded so far the identification of accurate biomarkers, especially for the early disease diagnosis (Nejad *et al.* 2013; Orru *et al.* 2012; Zahr *et al.* 2011).

One possibility to improve clinical diagnosis is to hybridize multi-modal neuroimaging datasets using multivariate pattern analysis, thereby enhancing the sensitivity for disease detection. Different MRI parameters have the capacity to sense the microscopic-level organization of brain tissues from different perspectives. For instance, changes in white or gray matter that limit the movement of water molecules in one or all directions of the microstructural space will change MRI measurements of water diffusivity (mean diffusivity, MD) or directionality (fractional anisotropy, FA). Similarly, lipid content in cell membranes, vasogenic edemas or accumulation of metals (i.e. iron) in cellular compartments may translate into detectable changes in those but also other MR parameters like T1- and T2-relaxation times (Bell-Temin *et al.* 2013; Dennis *et al.* 2014; Kong *et al.* 2012; McClain *et al.* 2011; Pfefferbaum & Sullivan 2005). The potential for multi-modal MRI has been already demonstrated in the characterization of brain gender dimorphisms in humans (Feis *et al.* 2013) and the identification of biomarkers in diagnosis for Alzheimer's disease (Klöppel *et al.* 2008; Magnin *et al.* 2009), mild cognitive impairment (Teipel *et al.* 2007) and recently in the discrimination of Parkinson disease from progressive supranuclear palsy (Salvatore *et al.* 2014) and differentiation between subtypes of primary progressive aphasia (Agosta *et al.* 2015).

In the present study we have combined multi-modal brain imaging in rats with probabilistic tissue segmentation and machine learning techniques to provide accurate readouts of alcohol-related brain damage and treatment-related brain responses. One major limitation of multi-modal approaches is the need to provide a few manually selected brain regions. Extended probabilistic segmentation methods of multi-spectral images allow labeling a small number of brain tissues such as gray matter, white matter, cerebrospinal fluid or sub classifications of them. However, these approaches require the incorporation of prior spatial information (Ashburner & Friston 2005; Fischl *et al.* 2002). Here we developed a new strategy to combine multiple parameters from different MRI modalities with no need for spatial information *a priori*, defining with a simple procedure a number of multi-modal regions of interest (mROIs). Using these mROIs we have built multi-modal imaging signatures of disease stage (MSDs) and explored its potential as biomarkers in an animal model of chronic excessive alcohol consumption, the Marchigian–Sardinian alcohol-preferring (msP) rat. This line was generated by selective breeding for high voluntary alcohol consumption. With a sustained high level of daily alcohol drinking leading to pharmacologically relevant blood alcohol concentrations, this animal model offers a useful tool for unraveling neural circuits associated with alcohol drinking (Ciccocioppo 2013; Ciccocioppo *et al.* 2006), and has been demonstrated its translational value to investigate naltrexone's suppressing effects on alcohol drinking (Egli 2005).

MATERIAL AND METHODS

Animal preparation

As an animal model for heavy alcohol drinking we used the alcohol-preferring Sardinian–Marchigian rat line (msP), which was created by selective breeding for high voluntary alcohol consumption (Ciccocioppo 2013; Ciccocioppo *et al.* 2006). A total of 18 msP rats (370–480 g) were used in these experiments. Rats were individually housed in transparent polycarbonate cages with bedding material, and a wooden stick and nesting material were given as enrichment. Rats had *ad libitum* access to food and water and were housed under controlled temperature (22 ± 2°C) and relative humidity (55 ± 10 percent) on a 12-hour light/dark cycle. Figure 1A summarizes the experimental design described below. The msP rats (imported from the breeding facility at the School of Pharmacy University of Camerino, Camerino, Italy) were individually housed for 30 days with access to two drinking bottles, one containing water and the other 10 percent (v/v) EtOH in water. Fluid consumption and animal weight were registered every 2–3 days concomitant with replacement of the bottles' content (Fig. 1B). After one month of two-bottle free-choice drinking regime, the EtOH-containing bottle was removed. At this point, msP animals ($n = 18$) were separated in two groups. In the first group animals proceeded into abstinence with daily medication with 2.5 mg/kg/day (i.p.) of naltrexone for one additional week ($n = 9$), a dose that has been previously shown to reduce alcohol consumption in msP rats (Ciccocioppo *et al.* 2007; Stopponi *et al.* 2013). In the second group, the abstinent animals were administered equivalent volumes of saline ($n = 9$).

All experiments were approved by the local authorities (IN-CSIC) and were performed in accordance with Spanish (law 32/2007) and European regulations (EU directive 86/609, EU decree 2001-486).

MRI experiments

Three multi-modal imaging sessions were scheduled longitudinally in msP rats, before and after 1 month of alcohol drinking (session t_1 and t_2, respectively), and after one week of abstinence in the absence or presence of naltrexone medication (t_3) (see above and Fig. 1A).

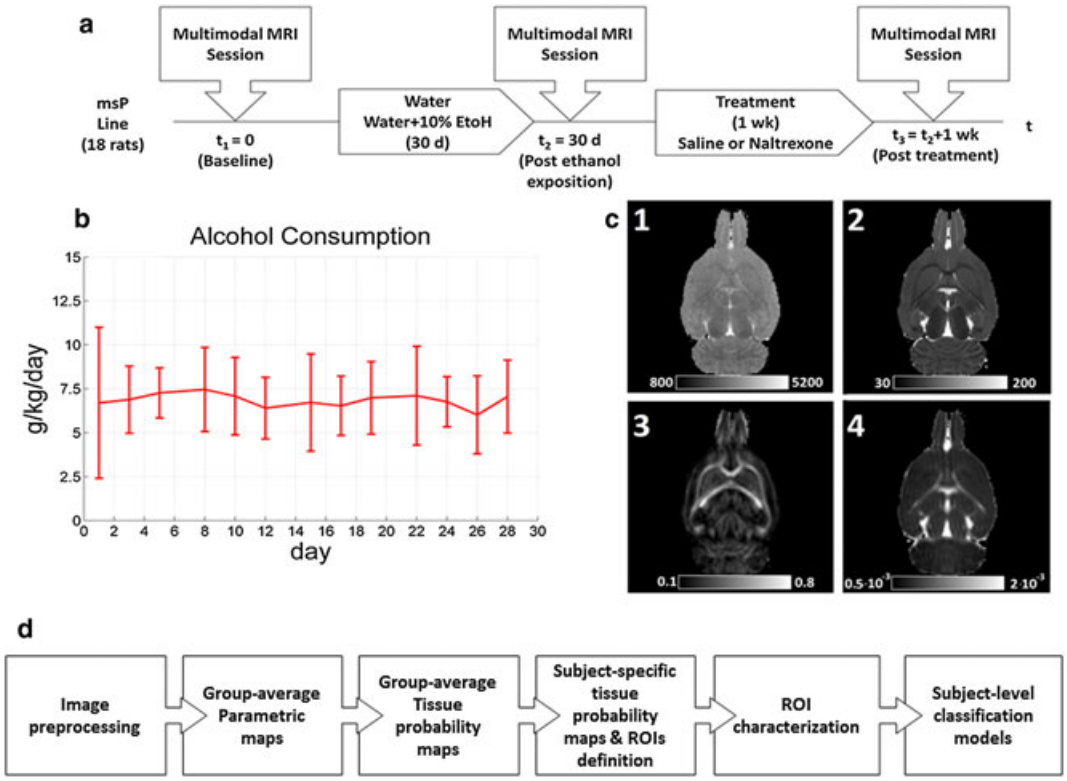

Figure 1 (a) Experimental design indicating the specific time points for treatment and imaging sessions performed in the longitudinal study of msP rats (upper diagram). (b) Level of alcohol consumption of the msP group. Data points represent the mean ± SEM of $n = 18$ animals. (c) Representative parametric maps of a msP subject before alcohol consumption: T1 (C.1) and T2 (C.2) maps in ms, FA (C.3) and MD (C.4) in mm^2/s. (d) Framework of the proposed procedure

Imaging experiments were performed under anesthesia. Anesthesia was induced with 4–5 percent isoflurane in oxygen (0.8–1 L/min) and animals secured on a custom-made holding apparatus with a tooth bar and a nose cone. During scanning, the isoflurane concentration was maintained at 1.2 percent, the body temperature was kept constant with a heating pad and physiologic parameters as oxygen saturation (SpO2), pulse distension, breathing and heart rate were monitored (MouseOx, Starr Life Sciences, Oakmont, PA, USA).

MRI experiments on rats were performed on a 7 T scanner (Bruker, BioSpect 70/30, Ettlingen, Germany) using a receive-only phase array coil with integrated combiner and preamplifier in combination with an actively detuned transmit-only resonator. Fourteen horizontal slices were planned for every subject (field of view [FOV] $= 32 \times 32\,mm^2$, matrix size $= 128 \times 128$, in-plane resolution $= 0.25 \times 0.25\,mm^2$, slice thickness $= 1$ mm). All imaging modalities were acquired with the same geometry. Two superior and two inferior slices were removed in the relaxometry maps in order to reduce the MRI acquisition time.

Diffusion Tensor Imaging (DTI) data was acquired using an EchoPlanar Imaging diffusion sequence, with 30 uniform distributed gradient directions, $b = 670\,s/mm^2$, with four non-diffusion weighted images, repetition time (TR) = 4000 ms and echo time (TE) = 23 ms.

T2 map images were acquired using a multi-slice multi-echo sequence (TR = 6000 ms, 30 echoes, min TE = 12 ms, increased TE = 12 ms). T1 map images were acquired using a Rapid Acquisition with Relaxation Enhancement (RARE) sequence with variable repetition time (TE = 12.61 ms, TR = [155 250 400 800 1600 3500 6000] ms).

T2-weighted images used for multi-modal image coregistration were acquired using a RARE pulse sequence (TR = 3800 ms, TE = 14 ms, number of averages = 6, FOV $= 32 \times 32\,mm^2$, 28 horizontal slices of 0.5 mm thickness and matrix size $= 256 \times 256$, resulting in $0.125 \times 0.125 \times 0.5\,mm^3$ voxel resolution).

Image pre-processing

Image analysis was performed using Statistical Parametric Mapping Software (SPM, Wellcome Trust Centre for Neuroimaging, Institute of Neurology, University College London, London, United Kingdom), FMRIB Software Library v5.0 (FSL, Analysis Group, FMRIB, Oxford, United Kingdom) and a collection of in-house programs developed using MATLAB 7.1 (The Mathworks Inc.,

Natick, MA, USA) and the free software environment for statistical computing and graphics R (R Foundation for Statistical Computing, Vienna, Austria).

Image data was converted from Bruker MRI format to Analyze format. All rat images were resized by a factor of 10 (to fit human brain dimensions and use default settings of FSL and SPM tools) (Biedermann *et al.* 2012). A voxel-by-voxel non-linear least squares fitting of T1 and T2 to a monoexponential signal decay curve ($S_0 e^{-TE/T2}$, $S = S_0\left(1 - e^{-TR/T1}\right)$, respectively) was performed at the relaxometry dataset. Parameters of the exponential signal decay were calculated and estimated by the non-linear least-squares fitting Trust-Region algorithm. T1 and T2 maps were corregistered to the T2-weighted images.

DTI was corrected for motion and fitted to local diffusion tensor using FSL. From the diffusion tensor components, FA and MD were determined. In order to correct the eddy current distortion, a subject-average of the basal images was non-linearly normalized to match the T2-weighted images corresponding to the same MRI session. FA and MD maps were spatially normalized using the previous spatial transformation. Despite other DTI-derived measures such as radial and longitudinal diffusivity maps ($\lambda_1/trace(D)$ and $(\lambda_2 + \lambda_3)/trace(D)$, respectively) might be more sensitive to diffusion changes in the brain tissue, they are strongly correlated with the anisotropy of the diffusion ellipsoid (described also by the FA) increasing features multi-collinearity. To trade-off between the minimum number of features (one additional parametric map would imply adding 49 new features) and diffusion ellipsoid description, we decided to describe water molecules motion by MD and FA measures only.

Despite motion correction in DTI dataset, residual artifacts might affect in a variety of ways the tensor reconstruction (Ling *et al.* 2012). To discard the possibility that residual artifacts may affect differentially the experimental groups, we used the alignment parameters (three rotations and three translations) of EPI dataset acquired during the scheduled MRI sessions (data not used for ROI definition and classification) to calculate the mean frame displacement (FD) (Power *et al.* 2012). Rotational parameters were transformed to millimeters (radius of the sphere 5 mm) and differences in FD between experimental groups formally tested. We found no main effects of movement parameters ($F = 1.562$, $p = 0.22$) nor interaction with the treatments ($F = 1.034$, $p = 0.36$). Therefore, we discarded any residual contribution of motion to the classification performance.

Subject structural images were used to create the group template and parametric maps using the SPM Diffeomorphic Anatomical Registration through Exponentiated Algebra or DARTEL procedure (Ashburner 2007). Briefly, for each subject, the structural image was first segmented and gray- and white-matter tissues collected to prepare the group template. Afterwards, FA, MD, T1 and T2 were non-linearly normalized using the flow field calculated in the DARTEL procedure to match the same anatomical space. An average of each parameter was extracted to define the group properties of the tissues. Using this multi-spectral information, a data-driven approach was implemented to define different regions of interest which share a similar multi-modal structure. Figure 1C shows the parametric maps generated in this analysis.

Multi-modal ROI (mROI) definition

In order to combine the multi-modal information derived from the MRI acquisition, different regions in the brain were defined using its microstructural and biochemical characteristics. For this purpose we tested two finite mixture models (FMM) using the Expectation Maximization (EM) algorithm (Dempster *et al.* 1977; Harville 1977). The Gaussian mixture model allows the overlapping of clusters (partial volume effect), handling uncertainty about cluster membership. The second FMM model, the finite Student's-*t* mixture model (Sfikas *et al.* 2008) alleviates the sensitivity of these methods to the presence of outliers, which results particularly efficient in brain imaging classification (Nguyen & Wu 2012).

We first combined penalized likelihood methods, such as Akaike Information Criterion (AIC) (Akaike 1974) and Bayesian Information Criterion (BIC) (Schwarz 1978), and cross-validation methods to estimate the dimensions and shape of the probability functions of the FMM (Smyth 2000). Additionally, the need for preprocessing data by the Cox–Box transformation (Box & Cox 1964) is evaluated (for a more detailed description of the methods see Supplementary Information). In order to select the multi-variate model which better fits the data in a reasonable time we used 10 percent of the data. For avoiding the convergence to local maximum, the EM algorithm is repeated 100 times with different initial parameters. Afterwards, and using the entire group-average parametric maps, the mixture of multi-variate distributions and transformation selection were estimated simultaneously using the approach proposed by Lo *et al.* (2009) and implemented in the R library 'flowClust'. Finally, probability maps of belonging to the different components in the model were calculated using the posterior probability.

To create a subject-specific version of the probability maps, tissue class templates in the segmentation approach implemented in SPM were replaced by the probability maps (Ashburner & Friston 2005) and projected to the individual anatomical space. The ROIs were defined using the largest posterior probability of belonging to a specific component in the subject-specific probability maps.

Feature extraction, ranking and support vector machine learning classification

We have used machine learning approaches to identify the metrics that accurately classify individuals according to the experimental conditions. In order to entirely describe the MRI parameters in each mROI, the unimodal texture was characterized by a set of seven histogram features sensitive to the data distribution within large brain areas, including the mean, standard deviation, median, first and third quartile, skewness and kurtosis. First order statistical features have been successfully used in glaucoma detection (El-Rafei *et al.* 2013) and Alzheimer disease (Magnin *et al.* 2009). Therefore, 28 features (seven histogram-derived measures extended to four MRI parametric maps) per subject and mROI were obtained. Only for displaying purposes, a principal component reduction is assessed. We selected support vector machine (SVM) to discriminate between different classes (Vapnik 2000) because it presents the advantage, over other machine learning approaches, to allow for non-linear effects, making use of radial basis or polynomial functions, among others, as a non-linear kernel.

The performance of the classification can be easily degraded by the presence of redundant features (Farahat *et al.* 2007; Kohavi & John 1997) and therefore the selection of variables that have discriminatory power is highly recommended (Mwangi *et al.* 2014).The discrimination between two classes was performed in a serial two-steps procedure. Firstly, features were ranked using the Random Forest (RF) algorithm (Breiman 2001; Genuer *et al.* 2010) and the error rate determined the importance of a given feature. The entire dataset was used as input in RF algorithm to provide a better generalization of those features with higher contribution to the differentiation of the disease stages. In order to reduce the effect of randomly choosing the variables, the algorithm was run 100 times with 1000 trees and 14 variables randomly sampled as candidates at each split. Then, SVM machine models were forwardly fed, namely starting from the highest relevant feature and adding next features in importance. The maximal performance evaluated by cross-validation accuracy defines the optimal dimensionality of the model.

Validation of the classification algorithm was performed by a cross-validation strategy. For this, the entire data set is partitioned into complementary subsets: the training and the testing set. The classification model is trained using the training set and the validation is performed on the test set. Specifically, we used *k*-fold cross validation with $k = 5$. The entire subset was split into five complementary subsets; four of them were used to train the SVM classifier and the remaining one to test the model (testing set). The testing set was shifted every run. In addition, the splitting of the data was repeated 100 times. Once variable importance has been estimated, models differing in the number of used variables are implemented. For this purpose, the model is fed with an increasing number of features on each iteration and evaluated in terms of accuracy, sensitivity and specificity. Sensitivity refers to the proportion of true positives correctly classified. Specificity refers to the proportion of true negatives correctly identified. The accuracy measurement represents the overall correct classifications. Furthermore, the area under the curve (AUC) of the receiver operating curve (ROC) was also used as a performance measure (Hanley & McNeil 1982). In brief, the AUC is a measure that describes how good the model is correctly assigning a participant in a group. To explore the potential overestimation of performance parameters by the inclusion of the entire dataset in the feature selection step, we also performed the RF in the inner loop of the cross-validation scheme, i.e. each training set was used to define a new ranking of features, and performance results were compared. In order to compare the performance of different models (univariate versus multi-variate with feature selection), a multi-variate model without previous feature selection is considered as the reference (null model). The complete analytical workflow is summarized in Fig. 1D.

To further validate the proposed algorithm (feature ranking, feature selection and prediction model), assignment in naïve and post-drinking data sets was randomly permuted (1000 times) to create the null-model distribution of the performance measures. Performance of the non-permuted-label classifier was tested against the null-model classifier performance distribution. Dimensionality model was set to the 38 highest-importance features representing the optimal number of features for the original labeling. Similarly, models differentiating saline versus naltrexone treatment under abstinence (34 most important features were the input to the classification stage) were validated.

RESULTS

During the 1-month period allocated for drinking in the two bottle free-choice paradigm msP animals consumed high levels of alcohol (6.8 ± 1.4 g/kg/day, mean ± SD) (Fig. 1B). All animals completed the three scheduled imaging sessions and data quality was comparable across sessions and animals (data not shown). The results of the multi-modal imaging study are presented as follows: (1) selection of the number of components and probabilistic functions of the FMM; (2) definition of different mROIs and their anatomical distribution; and (3) performance of the classifiers to discriminate between different stages in the AUD model.

Definition of the finite mixture model

A small sample of data (10 percent of the total number of observations) was used to estimate the optimal number of components for the mixture models (see Methods). The results of the BIC analysis for mixtures from 1 to 30 distribution functions are shown in Fig. S1. Both Gaussian and Student's *t* distribution models were tested, with and without Box–Cox transformation. An optimal statistical description of the data is obtained from seven components onwards, as indicated by the maximal BIC values, for both models (Fig. S1A). This result could be interpreted as an over fitting of the data when more than seven components are considered. However, this interpretation can be discarded because model fit is better for Student's *t* distribution than Gaussian also when the number of components is in the range of 1 to 7. This finding is consistent with previous reports stating that the use of longer-tailed distribution's *t* is more robust against the presence of outliers within the data (Chatzis & Varvarigou 2008). It is also important to highlight that the fitting is improved when the data has been previously transformed by the Box–Cox procedure (Lo *et al.* 2008) most likely because of the skewed distribution of the DTI data.

The probability maps of belonging to a distinct component of the seven selected above, here called mROIs, are provided in Fig. S1B. The mROIs demonstrated remarkably similar neuroanatomical demarcations with both methods, the mixture of Gaussian (Fig. S1B) and the Student's *t* distribution (Fig. S1B), illustrating the robustness of the approach. As can be seen in Fig. 2 and Fig. S1B, the variety of mROIs enrich any classical segmentation of brain tissues. While mROIs are dominated by either gray matter (i.e. mROI 1, 4 and 5), white matter (i.e. mROI 3) or cerebrospinal fluid (mROI 6), they represent subdivisions of these tissue classes with mROIs occupying differentiated cortical or subcortical territories (i.e. mROI 1 versus 4), and sometimes combining gray and white matter in virtue of their joint multi-modal properties (mROI 5). All mROIs show,

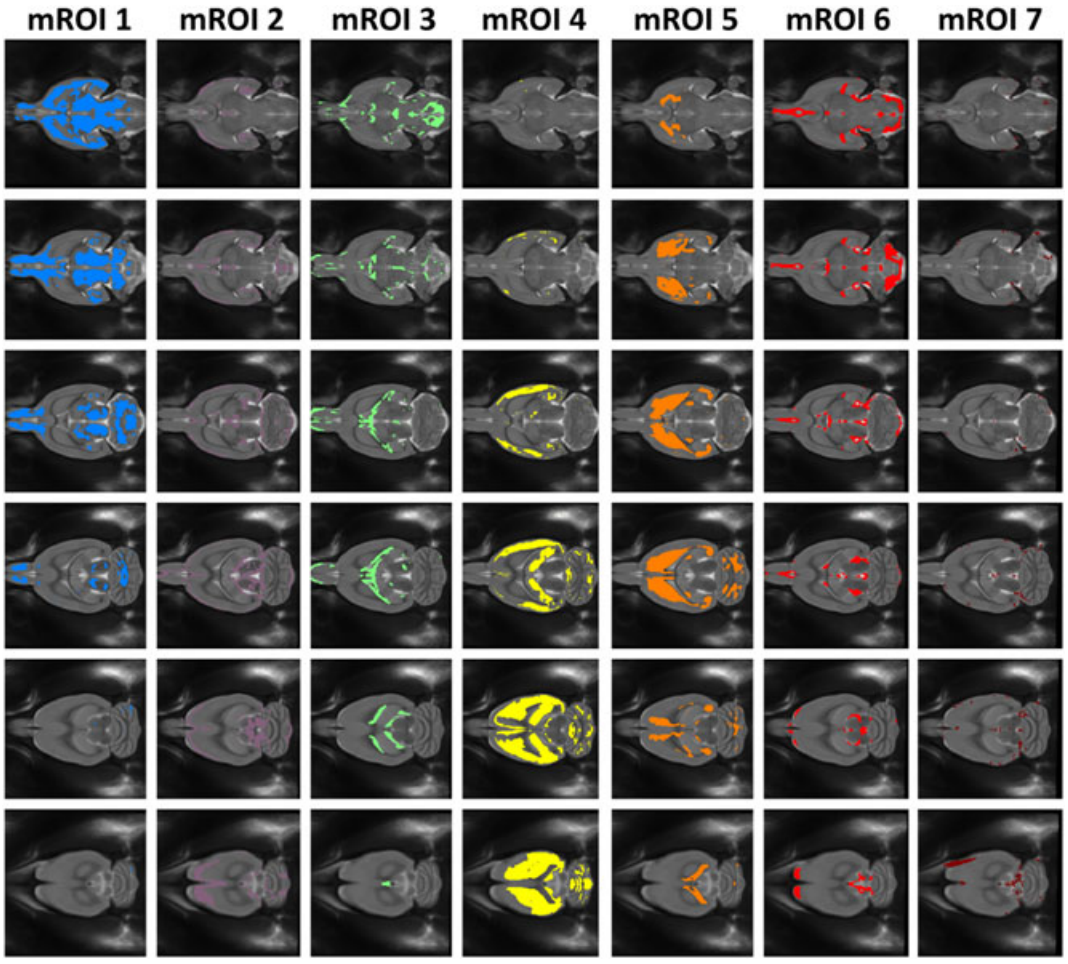

Figure 2 Multi-modal regions of interest (mROIs). Shown are six horizontal slices per mROI from more ventral (upper row) to dorsal positions (lower row) defined by thresholding the probability maps obtained with the Student's *t* mixture model. Note the bilateral anatomical symmetry of the components (mROIs). The color-coded probability maps for this and the Gaussian mixture models are shown in Fig. S1

however, well-defined midline symmetry, consistent with the bilateral (left–right) symmetry of the central nervous system. The slightly better BIC values obtained using the mixture of Student's *t* distribution (Fig. S1A) prompted us to adopt this model for the next steps of the analyses (Fig. 2).

As a first approximation to the multi-modal space across experimental conditions, the 196 classification features (corresponding to the seven measures in four MRI modalities in each of the seven mROIs selected, see methods for details) were reduced with principal component analysis. The two first components (19.8 and 12.7 percent of explained variance, respectively) are plotted in Fig. 3A. As can be seen, this simple analysis already identifies clusters of multi-modal observations that segregate at least a naïve state from a group of generic alcohol-related stages, providing a first visual validation of the experimental model and the power of multi-modal imaging to possibly differentiate between stages in AUDs.

Effects of alcohol consumption

For this first analysis we used the mROIs generated from msP animals before alcohol exposure and the same animals after 1 month of drinking. Excellent maximal performance of the classifiers in terms of sensitivity, specificity and accuracy is obtained with the proposed framework (Fig. 3C). The features mostly contributing to the model and, therefore, to discriminate between both stages (naïve versus alcohol drinking) are ranked in Fig. S2A. Alcohol drinking induced microstructural alterations in brain parenchyma mostly captured by MD and T2 relaxation times (Fig. 3C and S2). Optimal performance is obtained for classifications using 38 features (all of them derived from MD and T2 measures), remaining virtually constant thereafter. The area under ROC curve as a function of the number of features (Fig. S2C) further confirms the above results.

Comparing the above results with any univariate model (using single imaging modalities to identify alcohol-exposed subjects) demonstrates a significant reduction in all performance parameters (Table S1). Univariate T2 and MD models perform better than T1 and FA models, as expected from the ranking of features provided by the multi-variate analysis (Fig. S2A). Regarding the multi-variate models, the use of feature selection (RF) significantly increases its performance ($p < 0.001$). Both multi-variate models are plenty confident with AUC ≈ 1. Finally, we explored the presence of consistent subset of features able to discriminate naïve and exposed animals by evaluating the overfitting in our system (see methods). We determined that the inclusion of RF within the cross-validation scheme, this is preserving the

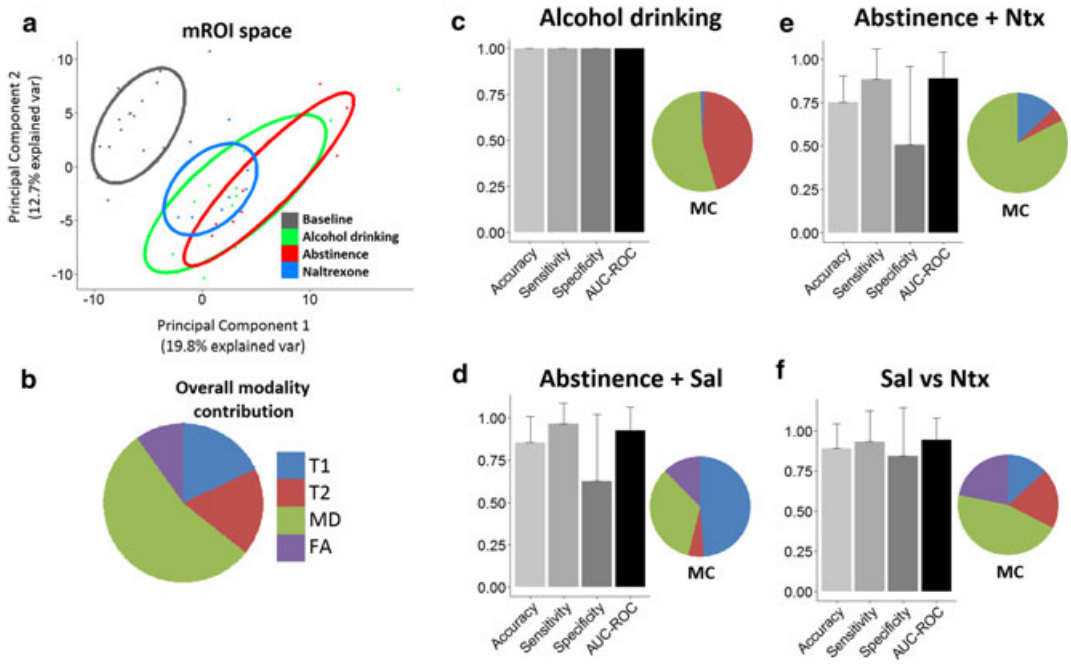

Figure 3 Classification performance. (a) Representation of the two first components obtained in the principal component analysis (PCA) of the 196 classification features. (b) Global modality contribution (MC) obtained averaging across classification models. (c–f) Performance of the optimal classifier (histogram) and MRI modality contribution (pie chart) for differentiating between the studied alcohol use stages: naïve versus alcohol drinking (c), drinking versus abstinence with saline (d), drinking versus abstinence with naltrexone (e) and saline versus naltrexone during abstinence (f)

independency of a test sample across both the RF and SVM steps, does not degrade the model performance (Fig. S3).

Overall from this analysis we can conclude that using multi-modal MRI information and machine learning methods the proposed framework correctly discriminates the occurrence of moderate levels of alcohol drinking with very high accuracy.

Abstinence as compared to its precedent period of alcohol drinking

The next logic step of our analysis was to investigate whether alcohol withdrawal or abstinence results in additional alterations in brain tissue producing a distinct multi-modal signature. For this analysis we used the same mROIs of the alcohol exposed animals in the previous section (alcohol condition), together with the mROIs of the same animals obtained one week after forced alcohol withdrawal (abstinence condition). The optimal performance of the classifier to differentiate between both conditions reached accuracy and sensitivity values above 85 percent with maximal specificity of 63 percent (Fig. 3D). The highest performance was obtained with the first 16 features (Fig. S4), and the feature ranking reveled that T1 and MD were the most relevant modalities contributing to the best classification (Fig. S4A). With chance level for the specificity of the model set at 50 percent, the 63 percent obtained here is considered low and suggests that the microstructural properties of brain tissues (as detected by multi-modal imaging) are not further altered in an early abstinence stage, as compared to the alcohol drinking state.

Univariate models analyzed for the alcohol-abstinence discrimination (Table S2) showed comparable performance of all singular modalities. However, the specificity of all of them was quite low. As found in the previous analysis, the best classification result is obtained with the multi-variate model combined with feature selection (Table S2).

Naltrexone treatment in alcohol abstinent rats

We next analyzed the effect of the opioid antagonist naltrexone, a clinically approved antirelapse medication. As before, the optimal performance of the model is shown in Fig. 3 and performance as a function of the number of features and feature identities are provided in Fig. S5. Optimal results are obtained for 16 features, with accuracy and sensitivity above 75 percent and model specificity at chance level (51 percent) (Fig. 3E and S5B). MD-derived features contribute maximally to the accuracy of the model (Fig. 3E and Fig. S5A), with absolute MD values initially enhanced by drinking ($p < 10^{-6}$, one-tailed paired *t*-test comparing average MD before and after drinking), returning towards the naïve state with naltrexone ($p < 0.03$, one-tailed *t*-test comparing average MD between saline and naltrexone treated abstinent animals). The recovery of MD under naltrexone treatment does not provide a sufficiently specific signature for the model to discriminate both conditions, suggesting a significant but partial recovery of alcohol-induced alterations in brain parenchyma induced by this antirelapse medication.

A specific multi-modal fingerprint for naltrexone versus saline medicated brains in abstinence

In the final analysis of the study we push the discriminative capacity of our method to differentiate between the two abstinent conditions. In the first, the abstinent animals receive daily treatment with the opioid receptor antagonist naltrexone, at a dose known to efficiently decrease drinking (Ciccocioppo *et al.* 2007; Stopponi *et al.* 2013) (naltrexone condition). In the second, animals received the same amount of solvent (saline). The results of the analysis demonstrate a very good performance of SVM to discriminate both conditions (Fig. 3F). Sensitivity, specificity and accuracy are above 84 percent when feature selection is performed with the complete dataset. The optimal number of features in this particular analysis is 34, with all imaging modalities contributing to them, being once again MD derived measurements especially well represented (Fig. S6A and Fig. 3F). However, contrary to the effect of alcohol exposure in naïve animals, in this case feature structures for accurate classification were less robust and the model degraded when the RF step was included in the cross-validation scheme (Fig. S7).

Univariate models show a significant reduction in almost all measures of classification performance when compared to multi-variate models (Table S4). The univariate MD model performance was the highest, as expected from the high ranking of MD-derive measures in Fig. S5A. Feature selection improved all performance indices and allows multi-variate models to reach an 89 percent of samples correctly classified with an AUC of 94.3 percent (Table S4).

Null model validation

The performance of our classification framework was tested against null models in which class labels were randomly permuted. In the first comparison, permuting the labels of naïve and exposed rats yielded a very low classification performance (accuracy = 0.52 (0.516–0.524), sensitivity = 0.526 (0.522–0.53), specificity = 0.53 (0.525–0.53), AUC-ROC = 0.7 (0.699–0.703)), with a

strong statistical significance in favor of the non-permuted model ($p < 0.001$ for all performance parameters). Similarly, the performance of SVM models trained to discriminate saline and naltrexone treated abstinent rats is strong and statistically higher than its corresponding (label permuted) null model (accuracy, $p < 0.001$; sensitivity, $p < 0.001$; specificity, $p = 0.004$; AUC-ROC, $p = 0.004$). The results obtained confirm the validity of the presented framework to discover feature pattern structures discriminating alcohol-related states in brain parenchyma.

DISCUSSION

The objective of this study was twofold. First, establishing a set of features or modalities from non-invasive neuroimaging capable of discriminate brain states in AUDs and, second, fitting SVM classifiers to quantify the degree of separability between them. The main findings are that: (1) robust and anatomically meaningful multi-modal signatures, here called mROIs, capturing the microstructural and biochemical properties of brain tissue can be defined by using MRI and finite mixture models; (2) the utility of these multi-modal signatures to characterize disease stages, here called MSDs, in a model of AUD has been demonstrated (Table 1); (3) the results show that even moderate phenotypes of alcohol drinking leave distinct recognizable signatures in brain tissues; (4) alterations in brain parenchyma induced by alcohol persist into abstinence, at least in its earlier stages; and (5) further changes in tissue microstructure are demonstrated after naltrexone treatment in alcohol abstinent animals, defining a potential treatment-related brain signature for this antirelapse medication.

Previous analytical approaches typically used in neuroimaging studies have considered a brain composition limited to three types of tissues (gray and white matter and cerebrospinal fluid) and combinations of them. However, in the present work we bring a new concept in tissue classification based on the combination of multiple microstructural properties of brain tissues that define novel tissue categories. This approach maximizes the potentialities of multi-modal MRI providing comprehensive and non-invasive descriptions of brain tissue without including prior spatial information. Another important aspect of our methodology that largely contributed to the success of the classifier is the full description of the different MRI parameters within every mROI by a number of first order statistical distribution measures. As has been demonstrated, the quantification of the textures of brain regions or simply histogram-derived feature extraction increases the classifier performance (El-Rafei *et al.* 2013; Magnin *et al.* 2009). Indeed, the first positions in the ranking of variable importance for correct classifications were usually occupied by features that described the statistical distribution of the parameter rather than its mean (Figs. S2–S7). Between the different modalities, our results highlight the contribution of MD to properly characterize alcohol-related brain changes, as well as treatment response. However, the use of complementary MRI modalities critically improved the accuracy of the models, confirming the analytic advantage of the multi-modal approach (Agosta *et al.* 2015; Dyrba *et al.* 2015; Pettersson-Yeo *et al.* 2014).

We have visually shown with a reduced representation of the multi-modal space that the acquired brain MRI parameters segregate according to the experimental conditions (Fig. 3A). This is especially clear for the naïve state which totally separates from the alcohol exposed conditions (no overlap between confidence ellipses in the PCA), in perfect agreement with the results of the classification model (100 percent of the cases are correctly assigned) (Fig. 3C). A challenging discrimination was found between alcohol-drinking and 1-week abstinence. The low specificity of the models to discriminate both conditions brings, however, neurobiological insight into the early phases of abstinence. Namely, that the microstructural changes in brain parenchyma induced by alcohol drinking are largely persistent after alcohol withdrawal in this relapse-prone state. Interestingly, although confidence ellipses of both abstinent conditions partially overlap, the simple PCA applied to the longitudinal

Table 1 Performance of the multi-variate models to differentiate between longitudinal conditions of msP rats.

	Accuracy	***Sensitivity***	***Specificity***	***AUC-ROC***
	Mean (95% C.I.)	*Mean (95% C.I.)*	*Mean (95% C.I.)*	*Mean (95% C.I.)*
Alcohol exposition	1.000 (1.000–1.000)	1.000 (1.000–1.000)	1.000 (1.000–1.000)	1.000 (1.000–1.000)
Abstinence	0.855 (0.837–0.874)	0.966 (0.951–0.981)	0.626 (0.577–0.675)	0.925 (0.908–0.942)
Abstinence in naltrexone	0.753 (0.734–0.771)	0.883 (0.862–0.905)	0.506 (0.450–0.562)	0.889 (0.871–0.908)
Naltrexone vs saline	0.890 (0.871–0.909)	0.932 (0.908–0.956)	0.844 (0.807–0.881)	0.943 (0.926–0.960)

Multi-variate SVM models using T1 and T2 relaxivity times, fractional anisotropy (FA) or mean water diffusivity (MD) after feature selection using the random forest (RF) algorithm.

imaging study already suggested a tendency for naltrexone treated subjects to return towards a baseline (naïve) state, while saline treated abstinent animals evolve towards a new state. This divergence between saline and naltrexone treated abstinent states was confirmed by our analytical model, with both conditions being correctly discriminated with high accuracy and specificity (Table 1 and Fig. 3F) when the optimal set of features is selected. When feature selection was included in the cross-validation scheme, however, classification performance dropped. This result could be explained by the decreased sample sizes accompanying this procedure or the more subtle changes in parenchymal microstructure between these conditions. In any case, from a neurobiological perspective, the obtained results selecting an optimal set of features demonstrate that the treatment with this antirelapse medication induces a physical change in brain parenchyma, and this change is mainly captured by alterations in MD. Whether it is robust enough to be used as a biomarker will require further investigations.

From a neurobiological perspective also, brain alterations characterized by MSDs provide quantitative information about tissue microstructure that may be also used to fill the gap between non-invasive clinical observations and neurobiological mechanisms. As mentioned in the introduction, a number of cellular changes have been correlated with alterations in acquired MRI parameters. For instance, changes in brain MD as predominantly found in our study have been frequently associated to neuroinflammatory processes (Alexander *et al.* 2007). In a recent longitudinal study of Wallerian degeneration contrasting MRI measurements with immunohistochemical evidence in cats (Qin *et al.* 2012), increased MD was clearly correlated with microglial activation and astrocytosis. A decrease in T2 signal has been also associated with astrocytic response in combined MRI and histopathological analysis in epileptic patients (Goubran *et al.* 2016), and was found in our study to contribute (second in importance after MD) to the successful discrimination between naïve and alcohol-exposed brains. Interestingly, neuroinflammation has been recently proposed as a mechanism of alcohol-related brain damage (He & Crews 2008; Qin & Crews 2012). If this were the case, the changes induced in the structure of brain parenchyma by a neuroinflammatory process, affecting the tortuosity and/or volume of the extracellular space, or inducing iron accumulation (Dennis *et al.* 2014; Kong *et al.* 2012; McClain *et al.* 2011; Pfefferbaum & Sullivan 2005), would help explain some of the individual MRI alterations found in our study. Furthermore, persistent alterations in neuroimmune signaling during chronic alcohol exposure have been suggested to underlie negative affective states, reduced neurogenesis and compromised frontal functions that could ultimately contribute to the development of alcohol addiction (Crews *et al.* 2011). Intriguingly, one postulated action of naltrexone is as anti-inflammatory (McLaughlin *et al.* 2013; Moslehi *et al.* 2014; Smith *et al.* 2011), reverting glial activation in the brain (Qin & Crews 2012). In this regard, the specific multi-modal signature found in our study for naltrexone treated brains, including a significant recovery of alcohol-induced MD and T2 changes, lends support to the neuroinflammatory hypothesis of alcohol-related brain damage. Furthermore, although changes in T1-relaxation times are affected by a number of factors, recent studies on an autoimmune model of multiple sclerosis have found an inverse correlation between this parameter and the extent of inflammation (Boretius *et al.* 2011), in good agreement with the increased T1 found under naltrexone medication and the postulated anti-inflammatory effects of this medication.

Other indirect factors potentially affecting tissue microstructure, as alcohol-triggered alterations in neurotransmission and neuronal physiology in general, with an impact on ionic gradients and energy metabolism, cannot be discarded. In this respect, we recently reported that chronic alcohol consumption by high alcohol preferring rats induced global effects on neuronal activity in many brain regions (Dudek *et al.* 2014). Importantly, and in line with the present results, changes in activity in that study persisted after one week of abstinence. Although the precise biological changes behind the multi-modal MRI alterations found in the present study are yet not known, the obtained results assure intensive research in that direction. Given the wide variety of alcohol consumption patterns in humans it will be important to demonstrate the ability of the framework to discriminate between different patterns of alcohol use in animal models that ensue a larger individual variability in drinking patterns and amounts, such as binging or chronic intermittent ethanol exposure (Carnicella *et al.* 2014; Crabbe *et al.* 2016; Meinhardt & Sommer 2015). Ultimately, the translational value of the proposed microstructural markers and their clinical utility has to be tested in human populations. If successful, an MRI based method to identify and stage early signs of alcohol-related brain pathologies would be of great clinical value, not only for early intervention, but also to enable investigations into the factors underlying the large individual heterogeneity of and susceptibility for such pathologies, for which the mechanisms are largely unknown (Zahr *et al.* 2011).

The fundamental goal of the present work was to provide a novel and robust approach to identify brain states based on the microstructural properties of the parenchyma with the vocation of providing a powerful diagnostic and prognostic framework. This possibility has been most clearly illustrated by the successful discriminations

of two subtle conditions, namely two abstinence states by virtue of the concomitant medication (either naltrexone or saline) in two groups of different animals. Within-animal comparisons also provided strong support to the analytical framework identifying a highly accurate and robust signature for brains exposed to a relatively short period of alcohol drinking, which persisted into early abstinence. Age differences in this within-animal comparisons were negligible (1 week for the abstinence versus alcohol drinking conditions and 4 weeks for the naïve versus drinking comparison), and we have further shown in previous studies that a period of 5 weeks in a group of rats of similar age resulted in no significant differences in volume brain morphometry (Hermann *et al.* 2012).

Concluding Remarks

We have presented an analytical framework that extracts microstructural information from multi-modal MRI to implement a novel concept of tissue segmentation based on mROIs. Combined with feature extraction and SVM learning models, these multi-modal signatures attained an excellent performance in the discrimination of disease stages and, for the first time to the best of our knowledge, to identify also a brain signature of treatment response. We propose that human MSDs could be valuable to assist accurate diagnosis and prognosis in neuropsychiatry, as well as to monitor treatment efficacy in individual patients.

Author Contribution

AC, PH, WS, DM and SC were responsible for the study concept. AC, DM and SC designed the multi-modal research strategy. AM and JPT carried out the experiments and MRI data collection. AC performed all data analysis. RC provided the experimental model. AC, DM and SC drafted the manuscript. RC, PH and WS provided critical revisions of the manuscript for intellectual content. All authors reviewed the manuscript and approved the final version for publication.

Acknowledgements

We are grateful to Begoña Fernández for her excellent technical assistance. Supported by grants from the Spanish MINECO to S.C. (BFU2015-64380-C2-1-R and PIM2010ERN-00679 as part of the Era-Net NEURON TRANSALC) and from the EU Horizon 2020 Program 668863-SyBil-AA grant, and to D.M. including FEDER funds under grant TEC2012-33778 and BFU2015-64380-C2-2-R. A.M. holds a studentship from the University of Edinburgh. The Instituto de Neurociencias is 'Centre of Excellence Severo Ochoa'.

References

Agosta F, Ferraro PM, Canu E, Copetti M, Galantucci S, Magnani G, Marcone A, Valsasina P, Sodero A, Comi G, Falini A, Filippi M (2015) Differentiation between subtypes of primary progressive aphasia by using cortical thickness and diffusion-tensor MR imaging measures. Radiology 276:219–227.

Akaike H (1974) A new look at the statistical model identification. IEEE Trans Automat Contr 19:716–723.

Alexander AL, Lee JE, Lazar M, Field AS (2007) Diffusion tensor imaging of the brain. Neurotherapeutics 4:316–329.

Ashburner J (2007) A fast diffeomorphic image registration algorithm. Neuroimage 38:95–113.

Ashburner J, Friston KJ (2005) Unified segmentation. Neuroimage 26:839–351.

Bell-Temin H, Zhang P, Chaput D, King MA, You M, Liu B, Stevens SM (2013) Quantitative proteomic characterization of ethanol-responsive pathways in rat microglial cells. J Proteome Res 12:2067–2077.

Biedermann S, Fuss J, Zheng L, Sartorius A, Falfan-Melgoza C, Demirakca T, Gass P, Ende G, Weber-Fahr W (2012) In vivo voxel based morphometry: detection of increased hippocampal volume and decreased glutamate levels in exercising mice. Neuroimage 61:1206–1212.

Boretius S, Escher A, Dallenga T, Wrzos C, Tammer R, Brück W, Nessler S, Frahm J, Stadelmann C (2011) Assessment of lesion pathology in a new animal model of MS by multiparametric MRI and DTI. Neuroimage 59:2678–2688.

Breiman L (2001) Random forests. Mach Learn 45:5–32.

Box GEP, Cox DR (1964) An analysis of transformations. J Roy Stat Soc B 26:211–52.

Bühler M, Mann K (2011) Alcohol and the human brain: a systematic review of different neuroimaging methods. Alcohol Clin Exp Res 35:1771–1793.

Carnicella S, Ron D, Barak S (2014) Intermittent ethanol access schedule in rats as a preclinical model of alcohol abuse. Alcohol 48:243–252.

Crabbe JC, Harris RA, Koob GF (2016) Preclinical studies of alcohol binge drinking. Ann N Y Acad Sci 1216:24–40.

Ciccocioppo R, Economidou D, Cippitelli A, Cucculelli M, Ubaldi M, Soverchia L, Lourdusamy A, Massi M (2006) REVIEW: genetically selected Marchigian Sardinian alcohol-preferring (msP) rats: an animal model to study the neurobiology of alcoholism. Addict Biol 11:339–355.

Ciccocioppo R, Economidou D, Rimondini R, Sommer W, Massi M, Heilig M (2007) Buprenorphine reduces alcohol drinking through activation of the nociceptin/orphanin FQ-NOP receptor system. Biol Psychiatry 61:4–12.

Ciccocioppo R (2013) Geneticallyselected alcohol preferring rats to model human alcoholism. Curr Top Behav Neurosci 13:251–269.

Chatzis S, Varvarigou T (2008) Robust fuzzy clustering using mixtures of Student's-t distributions. Pattern Recognit Lett 29:1901–1905.

Crews FT, Zou J, Qin L (2011) Induction of innate immune genes in brain create the neurobiology of addiction. Brain Behav Immun 25(Suppl 1):S4–S12.

Demirakca T, Ende G, Kämmerer N, Welzel-Marquez H, Hermann D, Heinz A, Mann K (2011) Effects of alcoholism and continued abstinence on brain volumes in both genders. Alcohol Clin Exp Res 35:1678–1685.

Dempster AP, Laird NM, Rubin DB (1977) Maximum likelihood from incomplete data via the EM algorithm. J Roy Stat Soc B 39:1–38.

Dennis CV, Sheahan PJ, Graeber MB, Sheedy DL, Kril JJ, Sutherland GT (2014) Microglial proliferation in the brain of chronic alcoholics with hepatic encephalopathy. Metab Brain Dis 29:1027–1039.

Dudek M, Abo-Ramadan U, Hermann D, Brown M, Canals S, Sommer WH, Hyytia P (2014) Brain activation induced by voluntary alcohol and saccharin drinking in rats assessed with manganese-enhanced magnetic resonance imaging. Addict Biol 20:1012–1021.

Dyrba M, Grothe M, Kirste T, Teipel SJ (2015) Multimodal analysis of functional and structural disconnection in Alzheimer's disease using multiple kernel SVM. Hum Brain Mapp 36:2118–2131.

Egli M (2005) Can experimental paradigms and animal models be used to discover clinically effective medications for alcoholism? Addict Biol 10:309–319.

El-Rafei A, Engelhorn T, Warntges S, Dorfler A, Hornegger J, Michelson G (2013) Glaucoma classification based on visual pathway analysis using diffusion tensor imaging. Magn Reson Imaging 31:1081–1091.

Farahat AK, Ghodsi A, Kamel MS (2007) An efficient greedy method for unsupervised feature selection. In: *Data Mining* (*ICDM*), *2011 IEEE 11th International Conference on*. IEEE. 161–170.

Fein G, Landman B, Tran H, McGillivray S, Finn P, Barakos J, Moon K (2006) Brain atrophy in long-term abstinent alcoholics who demonstrate impairment on a simulated gambling task. Neuroimage 32:1465–1471.

Feis DL, Brodersen KH, von Cramon DY, Luders E, Tittgemeyer M (2013) Decoding gender dimorphism of the human brain using multimodal anatomical and diffusion MRI data. Neuroimage 70:250–257.

Fischl B, Salat DH, Busa E, Albert M, Dieterich M, Haselgrove C, van der Kouwe A, Killiany R, Kennedy D, Klaveness S, Montillo A, Makris N, Rosen B, Dale AM (2002) Whole brain segmentation: automated labeling of neuroanatomical structures in the human brain. Neuron 33:341–355.

Genuer R, Poggi JM, Tuleau-Malot C (2010) Variable selection using random forests. Pattern Recognition Lett 31:2225–2236.

Goubran M, Bernhardt BC, Cantor-Rivera D, Lau JC, Blinston C, Hammond RR, de Ribaupierre S, Burneo JG, Mirsattari SM, Steven DA, Parrent AG, Bernasconi A, Bernasconi N, Peters TM, Khan AR (2016) In vivo MRI signatures of hippocampal subfield pathology in intractable epilepsy. Hum Brain Mapp 37:1103–1119.

Hanley JA, McNeil BJ (1982) The meaning and use of the area under a receiver operating characteristic (ROC) curve. Radiology 143:29–36.

Harville DA (1977) Maximum likelihood approaches to variance component estimation and to related problems. J Am Stat Assoc 72:320–338.

He J, Crews FT (2008) Increased MCP-1 and microglia in various regions of the human alcoholic brain. Exp Neurol 210:349–358.

Hermann D, Weber-Fahr W, Sartorius A, Hoerst M, Frischknecht U, Tunc-Skarka N, Perreau-Lenz S, Hansson AC, Krumm B, Kiefer F, Spanagel R, Mann K, Ende G, Sommer WH (2012) Translational magnetic resonance spectroscopy reveals excessive central glutamate levels during alcohol withdrawal in humans and rats. Biol Psychiatry 71:1015–1021.

Klöppel S, Stonnington CM, Chu C, Draganski B, Scahill RI, Rohrer JD, Fox NC, Jack CR Jr, Ashburner J, Frackowiak RSJ (2008) Automatic classification of MR scans in Alzheimer's disease. Brain 131:681–689.

Kohavi R, John GH (1997) Wrappers for feature subset selection. Relevance 97:273–324.

Kong LM, Zheng WB, Lian GP, Zhang HD (2012) Acute effects of alcohol on the human brain: diffusion tensor imaging study. Am J Neuroradiol 33:928–934.

Kril JJ, Halliday GM, Svoboda MD, Cartwright H (1997) The cerebral cortex is damaged in chronic alcoholics. Neuroscience 79:983–998.

Ling J, Merideth F, Caprihan A, Pena A, Teshiba T, Mayer AR (2012) Head injury or head motion? Assessment and quantification of motion artifacts in diffusion tensor imaging studies. Hum Brain Mapp 33:50–62.

Lo K, Brinkman RR, Gottardo R (2008) Automated gating of flow cytometry data via robust model-based clustering. Cytometry A 73:321–332.

Lo K, Hahne F, Brinkman RR, Gottardo R (2009) flowClust: a Bioconductor package for automated gating of flow cytometry data. BMC Bioinformatics 10:145.

Magnin B, Mesrob L, Kinkingnéhun S, Pélégrini-Issac M, Colliot O, Sarazin M, Dubois B, Lehéricy S, Benali H (2009) Support vector machine-based classification of Alzheimer's disease from whole-brain anatomical MRI. Neuroradiology 51:73–83.

Makris N, Oscar-Berman M, Jaffin SK, Hodge SM, Kennedy DN, Caviness VS, Marinkovic K, Breiter HC, Gasic GP, Harris GJ (2008) Decreased volume of the brain reward system in alcoholism. Biol Psychiatry 64:192–202.

McClain JA, Morris SA, Deeny MA, Marshall SA, Hayes DM, Kiser ZM, Nixon K (2011) Adolescent binge alcohol exposure induces long-lasting partial activation of microglia. Brain Behav Immun 25(Suppl 1):S120–S128.

McLaughlin PJ, Immonen JA, Zagon IS (2013) Topical naltrexone accelerates full-thickness wound closure in type 1 diabetic rats by stimulating angiogenesis. Exp Biol Med (Maywood) 238:733–743.

Meinhardt MW, Sommer WH (2015) Postdependent state in rats as a model for medication development in alcoholism. Addict Biol 20:1–21.

Moslehi A, Nabavizadeh F, Dehpour AR, Tavanga SM, Hassanzadeh G, Zekri A, Nahrevanian H, Sohanaki H (2014) Naltrexone attenuates endoplasmic reticulum stress induced hepatic injury in mice. Acta Physiol Hung 101:341–352.

Muller-Oehring EM, Jung YC, Pfefferbaum A, Sullivan EV, Schulte T (2015) The resting brain of alcoholics. Cereb Cortex 25:4155–68.

Mwangi B, Tian TS, Soares JC (2014) A review of feature reduction techniques in neuroimaging. -. Neuroinformatics 12:229–244.

Nejad AB, Madsen KH, Ebdrup BH, Siebner HR, Rasmussen H, Aggernaes B, Glenthoj BY, Baare WF (2013) Neural markers of negative symptom outcomes in distributed working memory brain activity of antipsychotic-naive schizophrenia patients. Int J Neuropsychopharmacol 16:1195–204.

Nguyen TM, Wu QMJ (2012) Robust Student's-t mixture model with spatial constraints and its application in medical image segmentation. IEEE Trans Med Imaging 31:103–116.

Orru G, Pettersson-Yeo W, Marquand AF, Sartori G, Mechelli A (2012) Using Support Vector Machine to identify imaging biomarkers of neurological and psychiatric disease: a critical review. Neurosci Biobehav Rev 36:1140–52.

Pettersson-Yeo W, Benetti S, Marquand AF, Joules R, Catani M, Williams SC, Allen P, McGuire P, Mechelli A (2014) An empirical comparison of different approaches for combining

multimodal neuroimaging data with support vector machine. Front Neurosci 8:189.
Pfefferbaum A, Sullivan EV (2005) Disruption of brain white matter microstructure by excessive intracellular and extracellular fluid in alcoholism: evidence from diffusion tensor imaging. Neuropsychopharmacology 30:423–432.
Qin L, Crews FT (2012) Chronic ethanol increases systemic TLR3 agonist-induced neuroinflammation and neurodegeneration. J Neuroinflammation 9:130.
Power JD, Barnes KA, Snyder AZ, Schlaggar BL, Petersen SE (2012) Spurious but systematic correlations in functional connectivity MRI networks arise from subject motion. Neuroimage 59:2142–2154.
Qin W, Zhang M, Piao Y, Guo D, Zhu Z, Tian X, Li K, Yu C (2012) Wallerian degeneration in central nervous system: dynamic associations between diffusion indices and their underlying pathology. PLoS One 7:e41441.
Rando K, Hong KI, Bhagwagar Z, Li CS, Bergquist K, Guarnaccia J, Sinha R (2011) Association of frontal and posterior cortical gray matter volume with time to alcohol relapse: a prospective study. Am J Psychiatry 168:183–192.
Salvatore C, Cerasa A, Castiglioni I, Gallivanone F, Augimeri A, Lopez M, Arabia G, Morelli M, Gilardi MC, Quattrone A (2014) Machine learning on brain MRI data for differential diagnosis of Parkinson's disease and Progressive Supranuclear Palsy. J Neurosci Methods 222:230–237.
Schwarz G (1978) Estimating the dimension of a model. Ann Stat 6:461–464.
Sfikas G, Nikou C, Galatsanos N (2008) Edge preserving spatially varying mixtures for image segmentation. *Computer Vision and Pattern Recognition, 2008. CVPR 2008. IEEE Conference* 1–7.
Smith JP, Bingaman SI, Ruggiero F, Mauger DT, Mukherjee A, McGovern CO, Zagon IS (2011) Therapy with the opioid antagonist naltrexone promotes mucosal healing in active Crohn's disease: a randomized placebo-controlled trial. Dig Dis Sci 56:2088–2097.
Smyth P (2000) Model selection for probabilistic clustering using cross-validated likelihood. Stat Comput 10:63–72.
Stopponi S, de Guglielmo G, Somaini L, Cippitelli A, Cannella N, Kallupi M, Ubaldi M, Heilig M, Demopulos G, Gaitanaris G, Ciccocioppo R (2013) Activation of PPARgamma by pioglitazone potentiates the effects of naltrexone on alcohol drinking and relapse in msP rats. Alcohol Clin Exp Res 37:1351–1360.
Teipel SJ, Born C, Ewers M, Bokde ALW, Reiser MF, Möller HJ, Hampel H (2007) Multivariate deformation-based analysis of brain atrophy to predict Alzheimer's disease in mild cognitive impairment. Neuroimage 38:13–24.
Vapnik V (2000) The Nature of Statistical Learning Theory. New York: Springer.
Whiteford HA, Degenhardt L, Rehm J, Baxter AJ, Ferrari AJ, Erskine HE, Charlson FJ, Norman RE, Flaxman AD, Johns N, Burstein R, Murray CJ, Vos T (2013) Global burden of disease attributable to mental and substance use disorders: findings from the Global Burden of Disease Study 2010. Lancet 382:1575–1586.
Wittchen HU, Jacobi F, Rehm J, Gustavsson A, Svensson M, Jonsson B, Olesen J, Allgulander C, Alonso J, Faravelli C, Fratiglioni L, Jennum P, Lieb R, Maercker A, van Os J, Preisig M, Salvador-Carulla L, Simon R, Steinhausen HC (2011) The size and burden of mental disorders and other disorders of the brain in Europe 2010. Eur Neuropsychopharmacol 21:655–79.
Zahr NM, Kaufman KL, Harper CG (2011) Clinical and pathological features of alcohol-related brain damage. Nat Rev Neurol 7:284–294.

SUPPORTING INFORMATION

Additional Supporting Information may be found in the online version of this article at the publisher's web-site:

Table S1 Performance of the univariate and multivariate models to differentiate between naïve and alcohol drinking msP rats.
Table S2 Performance of the univariate and multivariate models to differentiate between alcohol exposed and abstinent animals.
Table S3 Performance of the univariate and multivariate models to differentiate between alcohol exposed and abstinent animals treated with Naltrexone.
Table S4 Performance of the univariate and multivariate models to differentiate between two abstinence conditions with or without Naltrexone treatment.
Figure S1 Model definition. (A) Average BIC values with cross-validation procedure (k= 10 folds) from 1 to 30 components for both Gaussian and Student's t distributions with and without Box-Cox transformations. Dashed line indicates the optimal number of components in the model (N*=7) (B) Five slices of posterior probability maps (in columns) for belonging to 7 different components (rows). Gaussian (B.1) and Student's t (B.2) components are showed for comparison. Note the bilateral anatomical symmetry of the components (mROIs) and the remarkable similarity of the results obtained with both models.
Figure S2 Results of the implemented model to identify msP animals after one month of voluntary alcohol drinking. (A) Ranking of features according to their importance for model performance. (B) Sensitivity (green), specificity (blue) and accuracy (red) of the SVM model against the number of features. (C) Performance measured as the area under the ROC curve (AUC) of the model against the number of features.
Figure S3 Results of the implemented model to classify abstinent subjects according to Naltrexone or saline treatment including feature selection in the inner cross-validation loop. (A) Ranking of features according to their importance for model performance using the entire dataset (larger black dot) and the distribution of importance across cross-validation folds (boxplot). (B-E) Accuracy, Sensitivity, Specificity and AUC-ROC of the model against the number of features. Red line shows the performance of the SVM when feature selection is calculated for each fold and the blue line when the entire dataset is used as input in the RF algorithm.
Figure S4 Results of the implemented model to distinguish

between animals in a one month continuous drinking paradigm from the same subjects after a one week of forced abstinence. (A) Ranking of features according to their importance for model performance. (B) Sensitivity (green), specificity (blue) and accuracy (red) of the SVM model against the number of features. (C) Performance measured as the area under the ROC curve (AUC) of the model against the number of features.

Figure S5 Results of the implemented model to distinguish between animals in a one month continuous drinking paradigm from the same subjects after a one week of naltrexone treatment. (A) Ranking of features according to their importance for model performance. (B) Sensitivity (green), specificity (blue) and accuracy (red) of the SVM model against the number of features. (C) Performance measured as the area under the ROC curve (AUC) of the model against the number of features.

Figure S6 Results of the implemented model to classify abstinent subjects according to Naltrexone or saline treatment. (A) Ranking of features according to their importance for model performance. (B) Sensitivity (green), specificity (blue) and accuracy (red) of the SVM model against the number of features. (C) Performance measured as the area under the ROC curve (AUC) of the model against the number of features.

Figure S7 Results of the implemented model to identify msP animals after one month of voluntary alcohol drinking including feature selection in the inner cross-validation loop. (A) Ranking of features according to their importance for model performance using the entire dataset (larger black dot) and the distribution of importance across cross-validation folds (boxplot). (B-E) Accuracy, Sensitivity, Specificity and AUC-ROC of the model against the number of features. Red line shows the performance of the SVM when feature selection is calculated for each fold and the blue line when the entire dataset is used as input in the RF algorithm.